Available online at www.sciencedirect.com
SCIENCE DIRECT®
Journal of Solid State Chemistry 177 (2004) 4528–4534
JOURNAL OF SOLID STATE CHEMISTRY
www.elsevier.com/locate/jssc

Synthesis, optical properties and electronic structures of polyoxometalates $K_3P(Mo_{1-x}W_x)_{12}O_{40}$ $(0 \leqslant x \leqslant 1)$

F. Goubin[a], L. Guénée[a], P. Deniard[a], H.-J. Koo[b], M.-H. Whangbo[c], Y. Montardi[d], S. Jobic[a,*]

[a] *Institut des Matériaux Jean Rouxel, laboratoire de Chimie des Solides, UMR 6502 CNRS-Université de Nantes, 2 rue de la Houssinière, BP 32229, 44322 Nantes Cedex 3, France*
[b] *Department of Chemistry, Kyung Hee University, Seoul 130-701, South Korea*
[c] *Department of Chemistry, North Carolina State University, Raleigh, NC 27695-8204, USA*
[d] *Rhodia Electronics & Catalysis, 52 rue de la Haie Coq, 93308 Aubervilliers, France*

Received 2 July 2004; received in revised form 23 August 2004; accepted 27 August 2004
Available online 11 November 2004

Abstract

Various compositions of solid solutions $K_3P(Mo_{1-x}W_x)_{12}O_{40}$ $(0 \leqslant x \leqslant 1)$ were prepared using two solid state synthetic routes. The crystallite size was determined by linewidth refinements of X-ray diffraction patterns using the Warren–Averbach method, and the grain size distribution by laser scattering experiments. Optical properties were determined by diffuse reflectance measurements in the UV-visible range. The optical gap E_g was found to increase exponentially from ~2.5 to ~3.30 eV with increasing x, and is systematically shifted to a higher energy when the grain size decreases. The relation between E_g and x was analyzed by calculating the HOMO-LUMO gaps of the $[P(Mo_{1-x}W_x)_{12}O_{40}]^{3-}$ anions on the basis of tight-binding electronic structure calculations.

Keywords: Polyoxometalates; $K_3P(Mo_{1-x}W_x)_{12}O_{40}$ $(0 \leqslant x \leqslant 1)$; Grain size; Optical properties; HOMO-LUMO gaps

1. Introduction

Heteropolyoxometalates are polyanions of general chemical formula $[X_nM_pO_q]^{z-}$ [1], where M is mostly Mo or W and X is a main group or transition-metal atom. These anions are constructed from MO_6 octahedra encapsulating the X atom, which acts as a templating agent. Among them, the Keggin anions $[XM_{12}O_{40}]^{z-}$ [2] represent an important, representative class of heteropolyanions (X = Al, Si, P, Fe, Co, Cu and mostly M = Mo and W) and were extensively investigated because of their wide variety of properties and applications, including catalysis [3,4] and more recently medicine [5,6]. To our knowledge, however, these materials have never been systematically examined for their intrinsic optical properties, even though the absorption threshold of the Mo/W-based Keggin ions in solution are known to shift from the blue region of the electromagnetic spectrum (yellow hue) to the UV region (white hue) on going from Mo to W [7]. With a metal M in its highest oxidation state (d^0 electron configuration) and surrounded by six oxygen atoms, a strong absorption in the UV-visible range is expected with potential application as a yellow pigment or a UV absorber [8].

In the present work, we carry out a systematic study of the optical properties of Keggin-type $K_3P(Mo_{1-x}W_x)_{12}O_{40}$ $(0 \leqslant x \leqslant 1)$ compounds. Polyoxometalates are frequently prepared by acidifying a metalate solution (e.g., Na_2MoO_4) with H_3PO_4 [1] and then adding an organic salt (e.g., Bu_4NBr) to precipitate solid $A_3PM_{12}O_{40}$ (A = organic anion) materials. In the present work, we prepare the solid solutions

*Corresponding author. Fax: +33-2-40-37-39-95.
E-mail address: stephane.jobic@cnrs-imn.fr (S. Jobic).

0022-4596/$ - see front matter © 2004 Elsevier Inc. All rights reserved.
doi:10.1016/j.jssc.2004.08.046

$K_3P(Mo_{1-x}W_x)_{12}O_{40}$ ($0 \leqslant x \leqslant 1$) using two different methods, determine their crystal structures by powder XRD refinements, and measure their optical gaps by diffuse reflectance measurements. To explain the dependence of the absorption edges of $K_3P(Mo_{1-x}W_x)_{12}O_{40}$ ($0 \leqslant x \leqslant 1$) on the tungsten content x, we also carry out tight-binding electronic structure calculations for the anions $[P(Mo_{1-x}W_x)_{12}O_{40}]^{3-}$ ($0 \leqslant x \leqslant 1$) to obtain their HOMO-LUMO gaps.

2. Experimental

2.1. Synthesis

To ensure that we deal with intrinsic optical properties of $K_3P(Mo_xW_{1-x})_{12}O_{40}$, we prepared samples using two different methods. In the classical ceramic route (hereafter the "oxide route"), metal oxide MO_3, (Strem Chemicals, 99.9% for MoO_3 and Merck, 99% for WO_3), potassium carbonate (K_2CO_3, Aldrich, 99%) and dipotassium hydrogenophosphate (K_2HPO_4, Merck 99%) were intimately ground with a 10 wt% excess of K_2CO_3 and K_2HPO_4, and heated in air at 500 °C for 30 h in an alumina crucible. The soft chemistry route (hereafter the "acid route") employed a solid-state metathesis between a mineral acid hydrate $H_3PM_{12}O_{40}$, xH_2O (M = Mo, W) (Flucka) with a 6 wt% excess and potassium nitrate (KNO_3, Merck 99%) at 300 °C for 5 h. The resulting powder product was washed thoroughly with water to dissolve any remaining trace of acid impurity and then dried in air at 80 °C.

The acid route showed a higher chemical reactivity than does the oxide route, and is found appropriate for preparing pure samples of $K_3P(Mo_{1-x}W_x)_{12}O_{40}$ ($0 \leqslant x \leqslant 1$). In contrast, the oxide route led to better crystallized materials but its use was restricted to the range of $x = 0-0.6$ to obtain pure samples, because tungsten bronze impurities are systematically detected for $x > 0.6$. The color of the final product $K_3P(Mo_{1-x}W_x)_{12}O_{40}$ continuously varies with x, from yellow for $x = 0$ to white for $x = 1$. Moreover, $K_3PMo_{12}O_{40}$ prepared by the oxide route exhibits a bright yellow color (Fig. 1a), but that prepared by the acid route a pale yellow color (Fig. 1b). This trend is systematically observed for all Mo rich members of the $K_3P(Mo_{1-x}W_x)_{12}O_{40}$ series.

2.2. Analysis

The purity and crystallinity of samples were checked by XRD. The XRD patterns were collected using a Siemens D5000 diffractometer without monochromator (CuK-$L_{3,2}$, $\lambda = 1.540598$ and 1.544390 Å; reflection geometry; point detector with a 0.015° 2θ step; 2θ range = 10–100°). Structural refinements were performed with the Fullprof [9] software using the structure of $K_2(H_3O)PMo_{12}O_{40}$ as a model [10]. Tables 1 and 2 summarize results of the structural refinement as well as the compositions determined by Energy Dispersion X-ray Spectroscopy (on a JEOL JSM-5800LV scanning electron microscope coupled with a germanium PGT Prism detector).

The crystallite size was deduced by a Warren–Averbach analysis of the (200) and (400) diffraction peaks. The grain diameter distributions were deduced with a Beckman–Coulter LS 230 laser scattering particles size analyzer using the Mie model [11]. The refractive index of $K_3PMo_{12}O_{40}$ samples was found to be 2.15 according to the Gladstone Dale formula [12].

UV-visible diffuse reflectance spectra were recorded with a Varian Cary 5G spectrometer equipped with a Harrick Praying Mantis accessory and the WinUV software for computer controlling. The reflectance measurements were collected in the 200–600 nm range (i.e., from 2.07 to 6.20 eV) with a mirror sample as the reference for 100% reflectance. For pure molybdenum

Table 1
Cell parameters of $K_3P(Mo_{(1-x)}W_x)_{12}O_{40}$ solid solutions

$K_3P(Mo_{1-x}W_x)_{12}O_{40}$ composition			Synthetic route	Cell parameter a (Å)
Nominal	Refined	EDXS		
0			Oxide	11.5949(9)
			Acid	11.5881(7)
0.2	0.18(8)		Oxide	11.5948(4)
	0.20(4)	0.23	Acid	11.5910(3)
0.5	0.56(6)		Oxide	11.6011(4)
	0.44(4)	0.52	Acid	11.5986(3)
0.85	0.78(3)	0.86	Acid	11.6024(2)
0.90	0.86(3)	0.89	Acid	11.6025(4)
0.95	0.96(3)	0.93	Acid	11.6041(3)
1			Acid	11.6020(2)

Fig. 1. Color of $K_3PMo_{12}O_{40}$ samples prepared by: (a) the oxide route and (b) the acid route. The hue of a mixture $K_3PMo_{12}O_{40}$, polypropylene and polyethylene glycol heated at 180 °C is shown in (c).

Table 2
Atomic positions, isotropic atomic displacement parameters (Å^2) and reliability factors for $K_3PMo_{12}O_{40}$ (bold characters) and $K_3PW_{12}O_{40}$ (italic characters) synthesized by the oxide route and refined in the $Pn\bar{3}m$ space group

Atom	Site	x	y	z	B (Å^2)	τ
Mo	**24*k***	**0.4671(1)**	***x***	**0.2586(2)**	**0.97(4)**	**1**
W		*0.4671(2)*		*0.2577(4)*	*0.87(9)*	
O1	**24*k***	**0.6514(8)**	***x***	**0.007(1)**	**1.3(4)**	**1**
		0.649(3)		*0.010(5)*	*0.7(7)*	
O2	**24*k***	**0.0678(9)**	***x***	**0.768(1)**	**1.5(4)**	1
		0.068(3)		*0.762(6)*	*0.7(7)*	
O3	**24*k***	**0.1242(8)**	***x***	**0.543(1)**	**1.1(4)**	1
		0.126(3)		*0.538(5)*	*0.7(7)*	
O4	**8*e***	**0.326(1)**	***x***	***x***	**0.6(7)**	1
		0.323(3)			*0.7(7)*	
P	**2*a***	**¼**	**¼**	**¼**	**0.2(5)**	1
					0.7(7)	
K	**6*d***	**¼**	**¾**	**¾**	**2.7(3)**	1
					3(1)	

$R_p = 11\%$ $R_{wp} = 13\%$ $R_{Bragg} = 2.6\%$ $\chi^2 = 1.6$
$R_p = 12\%$ $R_{wp} = 14\%$ $R_{Bragg} = 6.0\%$ $\chi^2 = 3.3$

Table 3
Colorimetric coefficients for commercial yellow pigments and $K_3PMo_{12}O_{40}$

Compound	L	a	b	C_{ab}	h_{ab}
$PbCrO_4$	87.9	3.8	98.4	98.47	87.79
$BiVO_4$	90.4	−8.7	86.1	86.54	95.77
CdS	90.4	−6	95.1	95.29	93.61
$K_3PMo_{12}O_{40}$	86.7	2.08	85.19	85.22	91.41

samples, the Lab colorimetric coefficients (Table 3) were measured with a Pacific Spectrograd Colorimeter (sphere diameter of 150 mm). The stability of the material in contact with a polymer was also evaluated by heating polypropylene granules at 180 °C with 0.5 wt% of powder samples and 0.1 wt% of polyethyleneglycol.

2.3. Electronic structure calculations

$K_3P(Mo_{1-x}W_x)_{12}O_{40}$ ($0 \leqslant x \leqslant 1$) consists of isolated $[PMo_{12-x}W_xO_{40}]^{3-}$ anions, so we expect that the trend in the band gaps of $K_3P(Mo_{1-x}W_x)_{12}O_{40}$ ($0 \leqslant x \leqslant 1$) is well described by that in the HOMO-LUMO gaps of its $[PMo_{12-x}W_xO_{40}]^{3-}$ anions. Thus, extended Hückel tight-binding (EHTB) molecular calculations [13] were carried out for the $[PMo_{12-x}W_xO_{40}]^{3-}$ polyanions ($x = 0-12$) with all possible spatial distributions of Mo and W using the SAMOA package [14] and the atomic orbital parameters summarized in Table 4. The *d* orbitals of Mo/W and the *s*/*p* orbitals of O/P were represented by double-zeta Slater-type orbitals [15].

Table 4
Exponents ζ_i and valence shell ionization potentials H_{ii} of Slater-type orbitals χ_i used for extended Hückel tight-binding calculation[a]

Atom	χ_i	H_{ii} (eV)	ζ_i	C^b	ζ'_i	C'^b
Mo	5*s*	−8.34	1.955	1.00		
Mo	5*p*	−5.24	1.360	1.00		
Mo	4*d*	−10.50	3.954	0.4930	2.047	0.6458
W	6*s*	−8.26	2.281	1.00		
W	6*p*	−5.17	1.690	1.00		
W	5*d*	−10.37	4.151	0.5725	2.176	0.5799
O	2*s*	−32.3	2.688	0.7076	1.675	0.3745
O	2*p*	−14.8	3.694	0.3322	1.659	0.7448
P	3*s*	−18.6	2.367	0.5846	1.499	0.5288
P	3*p*	−14.0	2.065	0.4908	1.227	0.5940

[a] H_{ii}'s are the diagonal matrix elements $\langle \chi_i | H^{eff} | \chi_i \rangle$, where H^{eff} is the effective Hamiltonian. In our calculations of the off-diagonal matrix elements $H^{eff} = \langle \chi_i | H^{eff} | \chi_j \rangle$, the weighted formula was used. See: Ammeter, J.; Bürgi, H.-B.; Thibeault, J.; Hoffmann, R., *J. Am. Chem. Soc.* 100 (1978) 3686.
[b] Contraction coefficients used in the double-zeta Slater-type orbital.

3. Results and discussion

3.1. Structural and morphological aspects

Our XRD analysis of $K_3P(Mo_{1-x}W_x)_{12}O_{40}$ samples show that they are pure and crystallize in a cubic structure ($Pn\bar{3}m$) with cell parameters close to those of the isostructural $K_2(H_3O)PMo_{12}O_{40}$ compound [10]. The cell parameters and the chemical compositions of $K_3P(Mo_xW_{1-x})_{12}O_{40}$ are listed in Table 1 for $x = 0$, 0.2, 0.5, 0.85, 0.90, 0.95 and 1. (The sum of the occupancies of Mo and W was constrained to be 1 on the *M* sites in the structural refinements.) Only the atomic positions of the end-members $K_3PMo_{12}O_{40}$ and $K_3PW_{12}O_{40}$ are given in Table 2 for simplicity. Among the members in the $K_3P(Mo_{1-x}W_x)_{12}O_{40}$ series, no clear change is observed in their atomic positions because differences are within the usual experimental uncertainty. This is expected because the ionic radii of Mo^{6+} and W^{6+} are very similar (0.59 and 0.60 Å, respectively [16]). Thus, no steric strain is expected in the $K_3P(Mo_xW_{1-x})_{12}O_{40}$ solid solution.

The structure of $K_3PM_{12}O_{40}$ can be described as a cubic centered arrangement of discrete $[PM_{12}O_{40}]^{3-}$ anionic species (Fig. 2) counterbalanced by K^+ cations in octahedral sites. The polyanion $[PM_{12}O_{40}]^{3-}$ consists of four M_3O_{13} units made up of three MO_6 edge-sharing octahedra (O3–O4) (Fig. 2a). The M_3O_{13} units are linked to each other by corner-sharing (O1) to form an $[M_{12}O_{40}]$ cluster, the central cavity of which encases a phosphorus atom to form a PO_4 tetrahedron with four O4 oxygen atoms (Fig. 2b). In each MO_6 octahedron, the metal atom is displaced from the octahedral center toward the mono-coordinated O2 atom (i.e., the outermost oxygen atom of the Keggin polyanion).

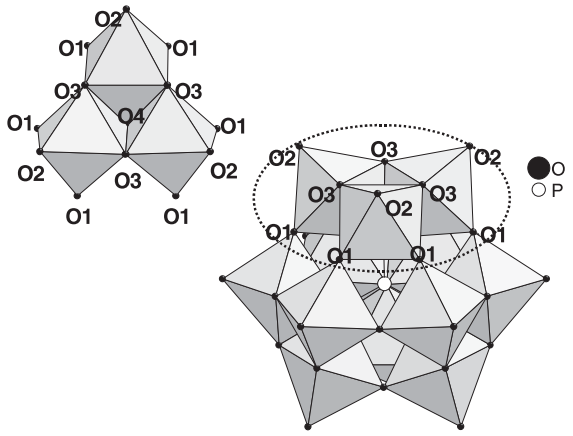

Fig. 2. (a) M_3O_{13} structural unit made up of three MO_6 octahedra, (b) $[PM_{12}O_{40}]$ polyanion made up of four M_3O_{13} units.

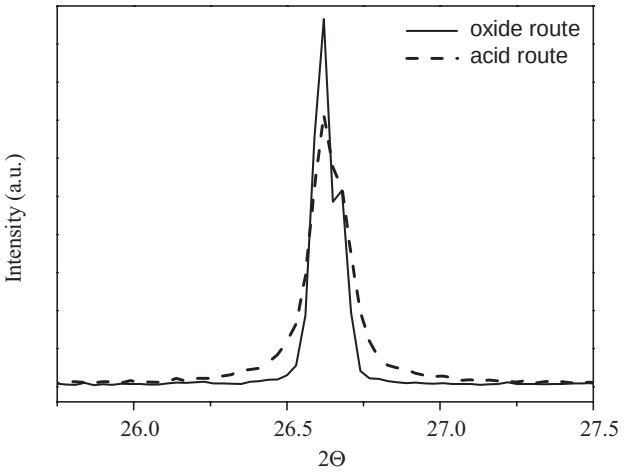

Fig. 3. Comparison of the linewidth of the (222) diffraction peak for $K_3PMo_{12}O_{40}$ powders prepared by the oxide route (solid line) and the acid route (dashed line).

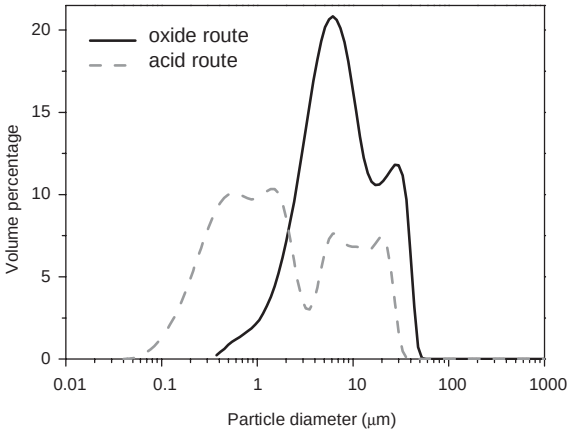

Fig. 4. Particle volume percentage as a function of particles size in $K_3PMo_{12}O_{40}$ samples prepared by the oxide route (solid line) and the acid route (dashed line).

The main structural feature differentiating the two synthetic routes is an isotropic line broadening of the diffraction peaks of the XRD patterns going from the oxide route to the acid route (Fig. 3). This may be due to a lower crystallinity (i.e., smaller crystallite sizes) and/or the existence of strains within the crystallites. To get some insight into this question, the crystallite size of $K_3PMo_{12}O_{40}$ samples was determined using the Warren–Averbach method [17,18] as implemented in the WINFIT software [19]. In this method, the peak shape is considered as the convolution of the incident X-ray beam wavelength distribution, the diffractometer resolution and intrinsic broadening of the materials due to sample imperfections (size and strain broadening). The first two can be measured and deconvoluted with a careful measurement of a standard (LaB_6 from NIST) under the same experimental conditions as used to collect the XRD pattern of the studied sample. Then, coherent size broadening and strain broadening can be separated, because the former and the latter depend on $1/\cos\theta$ and $tg\theta$, respectively. As a consequence, an accurate determination of the peak shape for several reflections within the same diffraction plane family allows one to separate between the crystallite size and the strain contributions.

Thus, following the classical procedure described elsewhere [17,18], the crystallite diameter was estimated to be about 340 Å for $K_3PMo_{12}O_{40}$ synthesized by the acid route (with a insignificant strain contribution to the HFWM, i.e., ~0.049%). In contrast, the oxide route leads to $K_3PMo_{12}O_{40}$ crystallite sizes large enough to avoid any line broadening compared with LaB_6, the coherent size domain being expected to be greater than 1000 Å. Laser scattering experiments carried out on $K_3PMo_{12}O_{40}$ samples yield the particle size distributions displayed in Fig. 4. The comparison of the volume percentage versus particle size shows a wider distribution of grain sizes for the acid route than for the oxide route (with diameters ranging from 0.05 to 30 μm and from 0.3 to 50 μm, respectively), and larger grains for the oxide route as expected. Note that the lowest values of the distributions agree well with the crystallite sizes determined by the Warren–Averbach method (i.e., 0.034 μm and higher than 0.1 μm). The smaller grain and crystallite size obtained by the acid route is probably related to the higher reactivity of this process compared with the oxide route.

3.2. Optical properties

3.2.1. Molybdenum phase

The reflectance spectra of $K_3PMo_{12}O_{40}$ samples synthesized by the oxide and acid routes are shown in Fig. 5. These spectra exhibit a large absorption band located in the UV and the violet regions of the

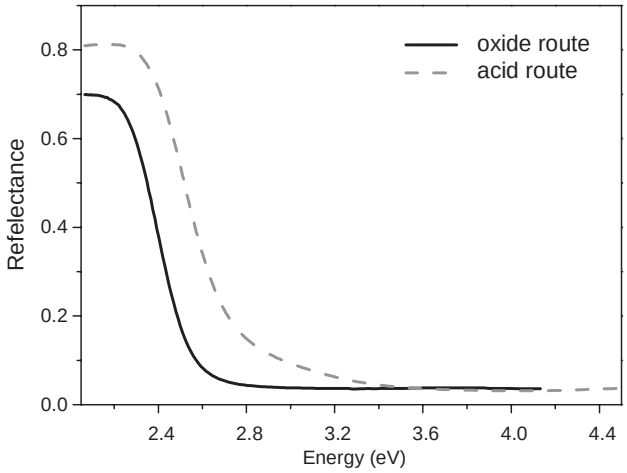

Fig. 5. Reflectance spectra of $K_3PMo_{12}O_{40}$ samples prepared by the oxide route (solid line) and the acid route (dashed line).

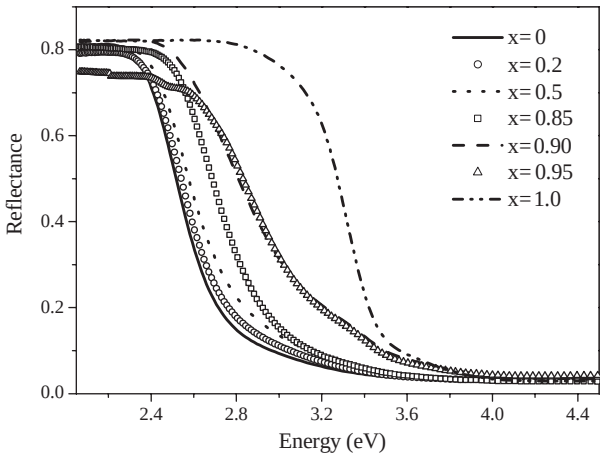

Fig. 6. Reflectance spectra of $K_3P(Mo_{(1-x)}W_x)_{12}O_{40}$ ($0 \leqslant x \leqslant 1$) samples prepared by the acid route.

electromagnetic spectrum, with a steep onset at 2.6 and 2.8 eV for the oxide and acid routes, respectively. These values are consistent with the colors of the $K_3PMo_{12}O_{40}$ samples (i.e., bright yellow for the oxide route, and pale yellow for the acid route) (Fig. 1). As already mentioned for Keggin ions in solution and other polyoxometalates [7], this absorption originates from the O $2p \rightarrow$ Mo $5d$ charge transfer.

The color variation for a given composition seems to follow the expected relationship between grain size and optical properties, i.e., the smaller the particles, the higher the absorption threshold becomes in energy. This is in part correlated with the energy dependant character of the scattering coefficient of powder samples [20,21] when the particle size is smaller than twice the length of the impinging electromagnetic wave (i.e., smaller than about 1 μm for a yellow compound).

Due to the bright hue of $K_3PMo_{12}O_{40}$ samples synthesized by the oxide route, the colorimetric Lab parameters were determined. As can seen in Table 3, the Lab parameters of $K_3PMo_{12}O_{40}$ are comparable to those of $PbCrO_4$, $BiVO_4$ and CdS. To probe its potential application as pigments, the powder was then embedded in polypropylene to evaluate its tinting strength. Unfortunately, the thus-obtained mixture exhibits a pale green color (Fig. 1c) originating from a molybdenum reduction process in contact with an organic medium at 180 °C, which is due to the ability of Keggin anions to become reduced without structural change. The generation of blue species associated with homonuclear charge transfers [22] leads to a green color by subtractive color mixing.

3.2.2. *Influence of Mo/W substitution*

Reflectance spectra were measured for all the samples of $K_3P(Mo_{1-x}W_x)_{12}O_{40}$ ($0 \leqslant x \leqslant 1$) prepared by the acid route (Fig. 6), while only three spectra were collected for

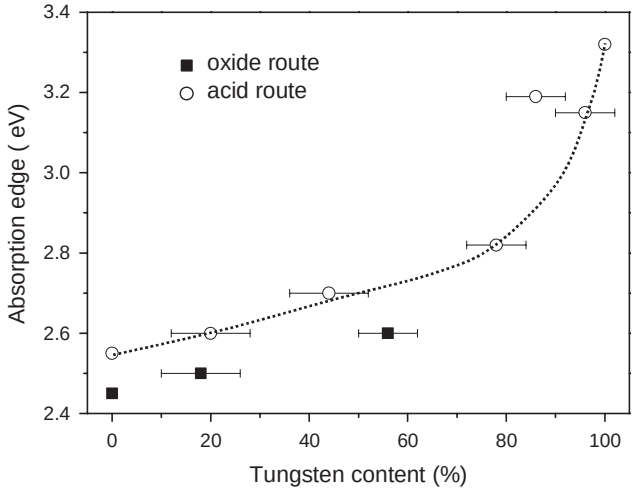

Fig. 7. Absorption threshold (eV) of $K_3P(Mo_{(1-x)}W_x)_{12}O_{40}$ ($0 \leqslant x \leqslant 1$) as a function of the tungsten content (%).

samples synthesized by the oxide route ($x = 0$, 0.2 and 0.5). The dependence of the absorption edges of $K_3P(Mo_{1-x}W_x)_{12}O_{40}$ ($0 \leqslant x \leqslant 1$) on the tungsten content x for the samples prepared by the two synthetic routes are presented in Fig. 7. The absorption edges, positioned at 2.45, 2.5, 2.6 eV for $x = 0$, 0.2 and 0.5 for the samples from the oxide route, and those ranging from 2.55 ($x = 0$) to 3.3 ($x = 1$) eV for the samples from the acid route, depend on the degree of crystallinity as already mentioned, and increases with increasing the tungsten content x (as determined by the Rietveld analysis). This shows that $K_3P(Mo_{1-x}W_x)_{12}O_{40}$ is not composed of $[Mo_{12}PO_{40}]^{3-}$ and $[W_{12}PO_{40}]^{3-}$ polyanions, but of $[Mo_{12-x}W_xPO_{40}]^{3-}$ ($0 \leqslant x \leqslant 12$) anions, and that the optical gap is tuned by changing the Mo/W ratio. This is in contrast to the finding for the $Y_{1-x}Ce_xPS_4$ solid solution, for which the Ce-$4f \rightarrow$ Ce-$5d$ absorption gap is independent of the Ce content x [23].

It should be pointed out that the absorption threshold of $K_3P(Mo_{1-x}W_x)_{12}O_{40}$ increases exponentially with increasing x (Fig. 7); the threshold increases slightly up to $x = 0.80$ and then varies much faster with increasing the tungsten content. To shed light on this trend, it is necessary to examine the electronic structure of the $[Mo_{12-x}W_xPO_{40}]^{3-}$ anions as a function of x, which is described in the next section.

3.3. Electronic structure

The electronic structure of Keggin ion was determined by Jansen et al. [24] using EHTB calculations, but the dependence of the electronic gap on the W/Mo ratio was not considered. To account for the intrinsic gap variation in $K_3P(Mo_{1-x}W_x)_{12}O_{40}$ $(0 \leqslant x \leqslant 1)$, we calculate the HOMO-LUMO gaps of the $[P(Mo_{1-x}W_x)_{12}O_{40}]^{3-}$ anions. Recently, first principles density functional theory electronic structure calculations have been reported for some Keggin anions [25–27]. These calculations predicted that the HOMO-LUMO gap is practically independent of the central ion, and increases from 2.06 to 2.50 eV and 2.84 eV for $[SiMo_{12}O_{40}]^{4-}$, C_{3v}-$[SiMo_3W_9O_{40}]^{4-}$ and $[SiW_{12}O_{40}]^{4-}$ anions, respectively.

For each composition x, all possible arrangements of the W and Mo arrangements in the anion were calculated. As an example, the three different configurations for $x = 0.5$ are given in Fig. 8, each triangle representing a MO_6 octahedron (M = Mo or W). No relaxation of the structural arrangement of the Keggin anion was considered because our XRD analysis showed no significant change in the structures of the $K_3P(Mo_{1-x}W_x)_{12}O_{40}$ series. The calculated HOMO-LUMO gaps as a function of x are summarized in Fig. 9. In terms of the smallest HOMO-LUMO gap for each value of x, the observed exponential increase of the absorption edge with increasing x is well reproduced. Therefore, the variation of the absorption threshold in the series $K_3P(Mo_{1-x}W_x)_{12}O_{40}$ reflects the intrinsic properties of their $[(Mo_{1-x}W_x)_{12}O_{40}]^{3-}$ anions.

It is noted from Fig. 9 that the HOMO-LUMO gaps of the $[(Mo_{1-x}W_x)_{12}O_{40}]^{3-}$ anions for a given x depend

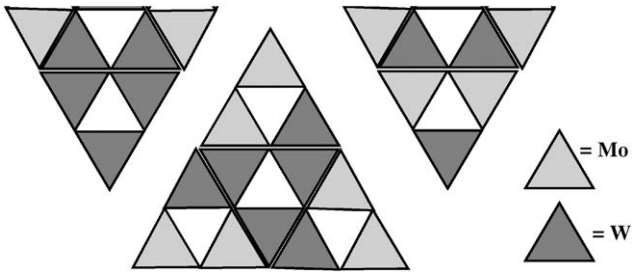

Fig. 8. Schematic representation of the three W atom arrangements used for the calculations of the HOMO-LUMO gaps of the $[P(Mo_{(1-x)}W_x)_{12}O_{40}]^{3-}$ anion for $x = 0.5$. The shaded and unshaded triangles represent the WO_6 and MoO_6 octahedra, respectively.

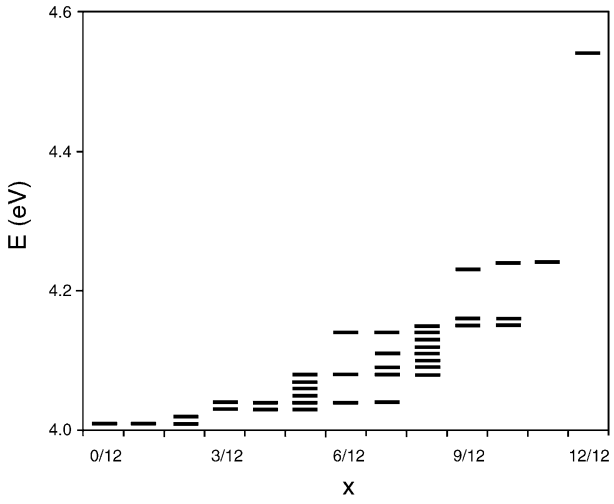

Fig. 9. HOMO-LUMO gaps calculated for the various W atom arrangements of the $[P(Mo_{(1-x)}W_x)_{12}O_{40}]^{3-}$ anions.

on the ordering of the W atoms. In $K_3P(Mo_{1-x}W_x)_{12}O_{40}$ samples for a given x, it is quite probable that all possible W atom orderings are present in their $[(Mo_{1-x}W_x)_{12}O_{40}]^{3-}$ anions. If so, the absorption band measured for a sample with a certain x would be the superposition of several absorption bands with different threshold energies. This explains why the reflectance spectra of solid solutions $K_3P(Mo_{1-x}W_x)_{12}O_{40}$ have a flatter absorption edge compared with those of the pure compounds $K_3PMo_{12}O_{40}$ and $K_3PW_{12}O_{40}$.

It is interesting to probe why the smallest HOMO-LUMO gap of the $[P(Mo_{1-x}W_x)_{12}O_{40}]^{3-}$ anion for each value of x increases strongly only in the region of $x = 1$. This observation stems essentially from the fact that the W 5*d* orbitals have a greater spatial extension than do the Mo 3*d* orbitals, and hence overlap better with the O 2*p* orbitals. In the *M*–O–*M* (*M* = Mo, W) bridges of $[(Mo_{1-x}W_x)_{12}O_{40}]^{3-}$, the O 2*p* orbitals make weak antibonding interactions with the *M d* orbitals in the LUMO, but weak bonding interactions with the *M d* orbitals in the HOMO [28]. Since the W 5*d* orbitals overlap better with the O 2*p* orbitals than do the Mo 3*d* orbitals, the energy of the highest-lying O 2*p* levels of the *M*–O–*M* bridges will increase in the order, W–O–W < W–O–Mo < Mo–O–Mo, while the lowest-lying *d*-block levels of the *M*–O–*M* bridges will increase in the order, Mo–O–Mo < W–O–Mo < W–O–W. Thus, to a first approximation, the HOMO-LUMO gap would be unaffected as long as the Mo–O–Mo bridges are present in the $[(Mo_{1-x}W_x)_{12}O_{40}]^{3-}$ anion. As the value of x approaches 1, the anion does not have the Mo–O–Mo bridges any more, so that the HOMO-LUMO gap is governed by the W–O–Mo bridges and is hence increased. Eventually, at $x = 1$, all the *M*–O–*M* bridges of the anion consist of the W–O–W bridges thereby leading to the largest HOMO-LUMO gap.

4. Concluding remarks

Of the two synthetic methods employed for preparing powder samples of $K_3P(Mo_{1-x}W_x)_{12}O_{40}$ ($0 \leqslant x \leqslant 1$), the acid route showed a higher chemical reactivity than does the oxide route, and leads to pure samples for the whole range of x. The acid route leads to a wider distribution of grain sizes and smaller grains than does the oxide route with a systematic blueshift. The optical gaps of solid solutions $K_3P(Mo_{1-x}W_x)_{12}O_{40}$ were determined as a function of the tungsten content x on the basis of diffuse reflectance measurements in the UV-visible range. With increasing x, the optical gap is found to increase exponentially from ~2.5 to ~3.30 eV, and this trend is well reproduced in terms of the HOMO-LUMO gaps calculated for the $[P(Mo_{1-x}W_x)_{12}O_{40}]^{3-}$ anions. The latter finding is well accounted for by considering how the HOMO and LUMO levels are affected by the W $5d$ and Mo $4d$ orbitals. $K_3PMo_{12}O_{40}$ samples prepared by the oxide route show the Lab parameters comparable to those of $PbCrO_4$, $BiVO_4$ and CdS, but lose their bright hue in an organic medium.

Acknowledgments

The work at NCSU was supported by the Office of Basic Energy Sciences, Division of Materials Sciences, US Department of Energy, under Grant DE-FG02-86ER45259.

References

[1] M. Pope, Heteropoly and Isopoly Oxometalates, Springer, New York, 1983.
[2] J.F. Keggin, Proceedings of the Royal Society of London, Series A 144 (1934) 75.
[3] T. Okuhara, N. Mizuno, M. Misono, Adv. Catalysis 41 (1996) 113.
[4] C.L. Hill, C.M. Prosser-McCartha, Coordination Chem. Rev. 143 (1995) 407.
[5] M. Pope, A. Müller, Polyoxometalates: from platonic solids to anti-retroviral activity, in: Topics in Molecular Organization and Engineering, vol. 10, Kluwer Academic Publishers, Dordrecht, 1994.
[6] S. Shigeta, S. Mori, E. Kodama, J. Kodama, K. Takahashi, T. Yamase, Antiviral Res. 58 (2003) 265.
[7] H. So, M. Pope, Inorganic Chem 11 (1972) 1441.
[8] G.M. Varga, E. Papaconstantiou, M. Pope, Inorganic Chem. 9 (1970) 667.
[9] J. Rodriguez-Carvajal, in: Abstract of the Satellite Meeting on Powder Diffraction of the XV Congress of the IUCr, Toulouse, France, 1990, p. 127.
[10] J.C.A. Boeyens, G.J. McDougal, J. van Smit, J. Solid State Chem. 18 (1976) 191.
[11] C.F. Bohren, D.R. Huffman, Absorption and Scattering of Light by Small Particles, Wiley-Interscience, New York, 1983.
[12] H.W. Jaffe, Am. Mineral. 41 (1956) 757.
[13] R. Hoffmann, J. Chem. Phys. 39 (1963) 1397.
[14] D. Dai, J. Ren, M.-H. Whangbo, Our calculations were carried out by employing the SAMOA (Structure and Molecular Orbital Analyzer) program package, http://chvamw.chem.ncsu.edu/.).
[15] E. Clementi, C. Roetti, Atomic Data Nucl. Data Tables 14 (1974) 177.
[16] R.D. Shannon, Acta Crystallogr. A 32 (1976) 751.
[17] B.E. Warren, X-ray Diffraction, Addison-Wesley, Reading, MA, 1969.
[18] B.E. Warren, B.L. Averbach, J. Appl. Phys. 23 (1952) 497.
[19] http://www.geol.uni-erlangen.de/html/software/winsoft.html.
[20] B. Cervelle, A. Bédidi, N. Flay, Photo-Interprétation 2 (1996) 35.
[21] G. Kortüm, Reflectance Spectroscopy, Springer, Berlin, 1969.
[22] T.J.R. Weakley, in: Structure and Bonding, vol. 18, Springer, Berlin, 1973, p. 131.
[23] G. Gauthier, Y. Klur, A. Pourpoint, S. Jobic, G. Ouvrard, R. Brec, D. Huguenin, P. Macaudière, Int. J. Inorganic Mater. 2 (2000) 717.
[24] S.A. Jansen, D.J. Singh, S.-H. Wang, Chem. Mater. 6 (1994) 146.
[25] J.M. Maestre, X. López, C. Bo, J.M. Poblet, N. Casañ-Pastor, J. Am. Chem. Soc. 123 (2001) 3749.
[26] X. López, C. Bo, J.M. Poblet, J. Am. Chem. Soc. 124 (2002) 12574.
[27] M. Poblet, X. López, C. Bo, Chem. Soc. Rev. 32 (2003) 297.
[28] E. Canadell, M.-H. Whangbo, Chem. Rev. 91 (1991) 965.